

# DA-Cal: Towards Cross-Domain Calibration in Semantic Segmentation

Wangkai Li , Rui Sun , Zhaoyang Li , Yujia Chen , Tianzhu Zhang , *Member, IEEE*

**Abstract**—While existing unsupervised domain adaptation (UDA) methods greatly enhance target domain performance in semantic segmentation, they often neglect network calibration quality, resulting in misalignment between prediction confidence and actual accuracy—a significant risk in safety-critical applications. Our key insight emerges from observing that performance degrades substantially when soft pseudo-labels replace hard pseudo-labels in cross-domain scenarios due to poor calibration, despite the theoretical equivalence of perfectly calibrated soft pseudo-labels to hard pseudo-labels. Based on this finding, we propose DA-Cal, a dedicated cross-domain calibration framework that transforms target domain calibration into soft pseudo-label optimization. DA-Cal introduces a Meta Temperature Network to generate pixel-level calibration parameters and employs bi-level optimization to establish the relationship between soft pseudo-labels and UDA supervision, while utilizing complementary domain-mixing strategies to prevent overfitting and reduce domain discrepancies. Experiments demonstrate that DA-Cal seamlessly integrates with existing self-training frameworks across multiple UDA segmentation benchmarks, significantly improving target domain calibration while delivering performance gains without inference overhead. The code will be released.

**Index Terms**—Uncertainty calibration, unsupervised domain adaptation, semantic segmentation.

## I. INTRODUCTION

Semantic segmentation, a fundamental computer vision task that assigns semantic labels to image pixels, enables comprehensive scene understanding. Despite significant advances with Deep Neural Networks (DNNs) [6], [9], [10], [37], these methods typically experience performance degradation when applied to novel target datasets due to distribution shifts between domains. This domain gap presents substantial challenges for network generalization. To address this limitation, Unsupervised Domain Adaptation (UDA) [55] are introduced by transferring knowledge from labeled source domains to unlabeled target domains, improving target performance without requiring additional annotations.

However, for segmentation networks in real-world applications, reliable uncertainty estimation is often as critical as accuracy, particularly in safety-critical scenarios like autonomous driving [3] and medical diagnosis [15], [31]. In these contexts, predictions must be both accurate and well-calibrated [21], [41]—where calibration refers to the alignment between network’s confidence and its actual accuracy. Despite current UDA methods significantly narrowing performance gaps between domains, we observe that they fail to show

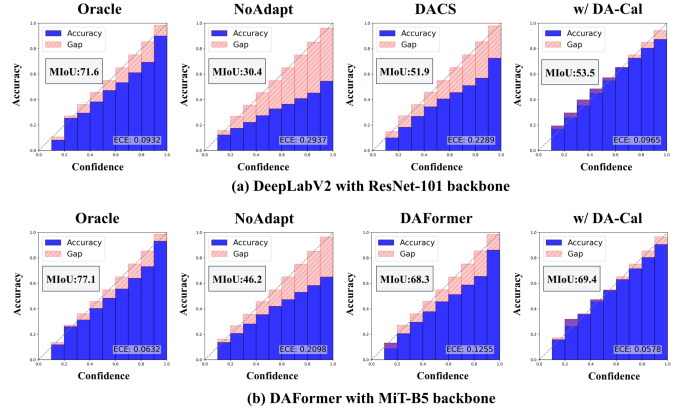


Fig. 1. **Reliability Diagrams** [43]. We observe that neural networks not only degrade in performance under cross-domain settings but also exhibit poor calibration. Although existing UDA methods, such as DACS [58] and DAFormer [25], significantly improve target-domain performance, they still struggle to produce well-calibrated predictions. When integrated with our proposed DA-Cal, these methods achieve consistently improved calibration, leading to more reliable confidence estimates.

corresponding improvements in calibration quality (Fig. 1). Moreover, state-of-the-art UDA approaches [26], [65] relying on self-training [34] may exacerbate confirmation bias, potentially degrading calibration further.

Current calibration methods fall into two categories: (1) Supervised IID calibration methods [21], [30], [42] adjust network outputs through post-hoc techniques by learning additional hyperparameters like temperature scaling. These approaches depend on labeled in-distribution validation sets, making them unsuitable for UDA task due to: a) the absence of labeled target domain data, and b) severe domain shifts that render source-calibrated networks ineffective for the target domain [13], [61]. (2) Domain-shift calibration methods [45], [61] use importance weighting [12] to establish relationships between target and source samples, addressing calibration under covariate shift. Additionally, [27] generates pseudo-target samples to simulate supervised calibration. Despite some progress, these methods are designed for classification tasks, and such sample-level modeling strategies are not guaranteed to work well for pixel-level semantic segmentation. *How to achieve cross-domain calibration in semantic segmentation remains an unresolved challenge.*

These challenges motivate us to explore a novel perspective for providing appropriate supervision signals to tackle unsupervised calibration in semantic segmentation. Our motivation stems from experimental observations of self-training-based UDA performance. When replacing argmax-based hard

The authors are with School of Information Science and Technology, University of Science and Technology of China (USTC), Hefei 230026, China. (e-mail: lwklwk, issunrui, lizhaoyang, yujia\_chen@mail.ustc.edu.cn; tzzhang@ustc.edu.cn). Corresponding author: Tianzhu Zhang.

pseudo-labels with softmax-based soft pseudo-labels, we observe significant performance degradation. This occurs because network predictions in the target domain are poorly calibrated. In Sec. III-B, we analyze that perfectly calibrated soft pseudo-labels should provide supervision equivalent to hard pseudo-labels. Based on this finding, we can reframe the calibration problem in the target domain into an optimization problem for soft pseudo-labels.

To this end, we propose a cross-domain calibration framework dedicated to semantic segmentation tasks, called DA-Cal, which transforms the target domain calibration problem into soft pseudo-label optimization involving two key designs to generate appropriate calibration temperatures for semantic segmentation outputs: (1) To convert soft pseudo-label optimization into temperature parameter optimization, we model it as a bi-level optimization problem, inspired by meta-learning [16], [36]. Specifically, we leverage bi-level optimization [47], [63] to establish the relationship between soft pseudo-labels and the UDA supervision of the segmentation network, thereby guiding the optimization direction of calibration temperature. The principle here is that if the network can produce perfectly calibrated pseudo-labels, it would also minimize the actual UDA supervision loss (i.e., the combined loss from source domain ground truth and target domain hard pseudo-labels). (2) To effectively apply this framework to semantic segmentation tasks, we first define the temperature parameter as a Meta Temperature Network (MTN) that can adaptively output pixel-level calibration temperatures, inspired by local temperature scaling [14]. Then, to effectively implement bi-level optimization, we employ complementary mixing strategies to generate different domain-mixed samples for the inner/outer optimization processes. This strategy effectively prevents MTN overfitting while mitigating domain discrepancies. Our framework is easy to integrate into existing self-training frameworks and effectively improves the calibration of UDA segmentation networks in the target domain. Additionally, DA-Cal can bring extra segmentation performance gains by introducing correctly calibrated soft pseudo-labels, without additional inference overhead.

Our contributions can be summarized as follows: (1) We identify a novel insight into UDA segmentation calibration by observing that performance degradation when using soft pseudo-labels is primarily caused by poor calibration, and analyze that perfectly calibrated soft pseudo-labels should provide supervision equivalent to hard pseudo-labels. (2) We propose DA-Cal, a dedicated cross-domain calibration framework that transforms target domain calibration into a bi-level optimization problem, featuring a Meta Temperature Network for pixel-level calibration temperatures and complementary domain-mixing strategies to prevent overfitting while addressing the unique challenges of semantic segmentation calibration. (3) Our method seamlessly integrates with existing self-training UDA frameworks, improving both calibration quality and segmentation performance in the target domain without additional inference overhead, demonstrating effectiveness across various UDA segmentation benchmarks.

## II. RELATED WORK

### A. Domain Adaptive Semantic Segmentation

Unsupervised domain adaptation (UDA) for semantic segmentation addresses the costly pixel-wise annotation problem by transferring knowledge from labeled source domains to unlabeled target domains. Current approaches primarily follow two paradigms: adversarial training-based methods [8], [17], [56], [59] that align feature distributions through domain discriminators, and self-training-based methods [1], [25], [35], [58] that generate pseudo-labels within teacher-student frameworks. The latter has become dominant due to the domain-robustness of Transformers [2], with researchers developing various strategies to improve pseudo-label quality, such as entropy minimization [7] and consistency regularization [26]. Recent advances further expand the field: DTS [29] leverages different mixing strategies in a dual teacher-student framework, CDAC [60] enforces consistency in attention mechanisms, and RTea [71] incorporates structural information as additional supervision. Other innovative approaches include diffusion-based image translation [46], integration of distillation with self-training [54], utilization of domain-agnostic text embeddings [39], and architectural innovations to learn domain-invariant representations [24], [65]. While these methods have significantly improved segmentation accuracy across domains, the calibration quality of UDA models remains largely unexplored.

### B. Uncertainty Calibration

Calibration methods ensure model predictions align with actual correctness likelihoods, evolving from binary classification [48], [69] to multi-class settings through approaches like matrix scaling, vector scaling, and temperature scaling [21]. Temperature scaling has become predominant due to its simplicity and effectiveness, with extensions like ATS [42] addressing small validation dataset challenges and BTS [30] employing bin-wise scaling with data augmentation. For semantic segmentation specifically, researchers have developed spatial-aware calibration techniques such as local temperature scaling [14] to capture pixel-level heterogeneity, model ensembling with segment-level metrics [40], and adversarial training of stochastic networks [32]. However, these supervised calibration methods rely on labeled validation data and in-distribution assumptions, making them unsuitable for unsupervised domain adaptation scenarios where labeled target data is unavailable and domain shifts are significant. To address this gap, domain-shift calibration approaches have emerged, including methods that use source validation sets as domain-generalized targets [53], [57], [72], importance weighting techniques [22], [45], [61] to relate target and source samples, and multi-source domain utilization [19], [67]. Despite this progress, most existing methods are designed for classification tasks, and their sample-level modeling strategies do not effectively translate to semantic segmentation where pixel-level calibration is required, leaving cross-domain calibration in semantic segmentation an unresolved challenge.

### III. METHOD

#### A. Preliminaries

**Self-Training for UDA.** In unsupervised domain adaptation for semantic segmentation, the network is simultaneously trained on labeled source domain data and unlabeled target domain data. Specifically, the source domain can be denoted as  $D_S = (x_i^S, y_i^S)_{i=1}^{N_S}$ , where  $x_i^S \in X_S$  represents an image with  $y_i^S \in Y_S$  as the corresponding pixel-wise one-hot label covering  $C$  classes. Similarly, the target domain is  $D_T = (x_i^T)_{i=1}^{N_T}$ , which shares the same label space but has no access to the target labels. A self-training-based UDA pipeline consists of a supervised branch for the source domain and an unsupervised branch for the target domain. For the supervised branch, the loss  $\mathcal{L}^s$  can only be calculated on the source domain to train a neural network  $f_\theta$ :

$$\mathcal{L}^s = \frac{1}{N_S} \sum_{i=1}^{N_S} \frac{1}{HW} \sum_{j=1}^{H \times W} \ell_{ce}(f_\theta(x_{ij}^S), y_{ij}^S), \quad (1)$$

where  $\ell_{ce}$  denotes the cross-entropy loss. The unsupervised branch introduces a teacher-student framework to generate pseudo-labels  $\hat{y}_{ij}^T = \arg\max(g_\phi(x_{ij}^T))$  with the teacher network  $g_\phi$  for the target domain:

$$\mathcal{L}^u = \frac{1}{N_T} \sum_{i=1}^{N_T} \frac{1}{HW} \sum_{j=1}^{H \times W} q(p_{ij}) \ell_{ce}(f_\theta(x_{ij}^T), \hat{y}_{ij}^T), \quad (2)$$

where  $q(p_{ij})$  is a quality estimate conditioned on confidence  $p_{ij} = \max(g_\phi(x_{ij}^T))$  for pseudo-labels, which improves as network accuracy increases [25]. After each training step, the teacher network  $g_\phi$  is updated with the exponentially moving average of the weights of  $f_\theta$ . The overall objective function is a combination of supervised and unsupervised losses:  $\mathcal{L} = \mathcal{L}^s + \mathcal{L}^u$ .

**Temperature Scaling for Calibration.** Temperature Scaling [21] is proposed as a simple extension of Platt scaling [48] for post-hoc probability calibration in multi-class classifications. Specifically, temperature scaling estimates a single scalar parameter  $\mathcal{T} \in \mathbb{R}^+$ , i.e., the temperature, to calibrate probabilities:  $\hat{p} = \max_{c \in C} \sigma_{SM}(\mathbf{z}/\mathcal{T})^{(c)}$ , where  $\hat{p}$  is the calibrated probability. For semantic segmentation tasks, temperature scaling can be directly extended by estimating one global parameter  $T \in \mathbb{R}^+$  for all pixels/voxels of all images:

$$\hat{p}(x_{ij}, \mathcal{T}) = \max_{c \in C} \sigma_{SM}(f_\theta(x_{ij})/\mathcal{T})^{(c)}. \quad (3)$$

The optimal value for  $\mathcal{T}$  is obtained by minimizing the negative log-likelihood (NLL) with respect to a hold-out validation dataset:

$$\mathcal{T}^* = \arg \min_{\mathcal{T}} \left( - \sum_{i=1}^N \sum_{j=1}^{H \times W} \log(\sigma_{SM}(f_\theta(x_{ij})/\mathcal{T})^{(y_{ij}^S)}) \right) \quad (4)$$

s.t.  $\mathcal{T} > 0$ .

However, temperature scaling in this way assumes that each image has the same distribution (i.e., the same temperature,  $\mathcal{T}$ , for all images), which is unrealistic, especially in domain adaptation settings where source and target distributions differ significantly.

#### B. Motivation

In domain adaptation classification, we analyze the relationship between hard and soft pseudo-labels. Let  $f_\theta(x)$  be a network that outputs logits for an input  $x$ , and  $\sigma_{SM}(f_\theta(x)/\mathcal{T})$  be the softmax probabilities after temperature scaling with parameter  $\mathcal{T}$ . For a perfectly calibrated network, the predicted probability for each class should match its empirical accuracy:

$$P(\text{correct} | \sigma_{SM}(f_\theta(x)/\mathcal{T})^{(c)} = p) = p \quad \forall p \in [0, 1], \forall c \in C. \quad (5)$$

This means when the network predicts class  $c$  with confidence  $p$ , it should be correct exactly  $p$  proportion of the cases. Equivalently, in terms of posterior probabilities, a perfectly calibrated network satisfies:

$$\sigma_{SM}(f_\theta(x)/\mathcal{T})^{(c)} = P(y = c | x) \quad \forall c \in C. \quad (6)$$

We now compare the losses for soft/hard pseudo-labels.

a) *Soft Pseudo-Labels.*: When using soft pseudo-labels, the cross-entropy loss is:

$$\mathcal{L}_{\text{soft}} = - \sum_{c \in C} \sigma_{SM}(f_\theta(x)/\mathcal{T})^{(c)} \log(\hat{p}^{(c)}). \quad (7)$$

b) *Hard Pseudo-Labels.*: For hard pseudo-labels, we select the class with the highest confidence:  $\hat{y} = \arg \max_{c \in C} \sigma_{SM}(f_\theta(x)/\mathcal{T})^{(c)}$ , yielding the loss:

$$\mathcal{L}_{\text{hard}} = - \log(\hat{p}^{(\hat{y})}). \quad (8)$$

For a perfectly calibrated network, the expected hard pseudo-label loss equals the soft pseudo-label loss:

$$\mathbb{E}[\mathcal{L}_{\text{hard}}] = \sum_{c \in C} P(y = c | x) \cdot (- \log(\hat{p}^{(c)})) = \mathcal{L}_{\text{soft}}. \quad (9)$$

Thus, under perfect calibration, soft and hard pseudo-labels are equivalent. However, our experiments reveal severe performance degradation when using only soft pseudo-labels in UDA. This degradation stems from miscalibration of the soft pseudo-labels. Therefore, we can reformulate the calibration problem as an optimization task aimed at improving soft pseudo-label quality.

#### C. The DA-Cal Framework

To address pseudo-label miscalibration in domain adaptation, we propose DA-Cal, a bi-level optimization framework (illustrated in Fig. 2). DA-Cal simultaneously optimizes the segmentation network and the calibration network inspired by meta-learning. It consists of:

- *Inner optimization*, which learns optimal temperature calibration parameters.
- *Outer optimization*, which updates the segmentation network using calibrated pseudo-labels.

**Meta Temperature Network (MTN).** We introduce a Meta Temperature Network (MTN) to predict pixel-wise temperature values for calibration. The network simply consists of stacked Conv-BatchNorm-ReLU blocks for efficient processing. The MTN takes two inputs: the original image and the logits output by the segmentation network, which are concatenated along the channel dimension. The MTN outputs a

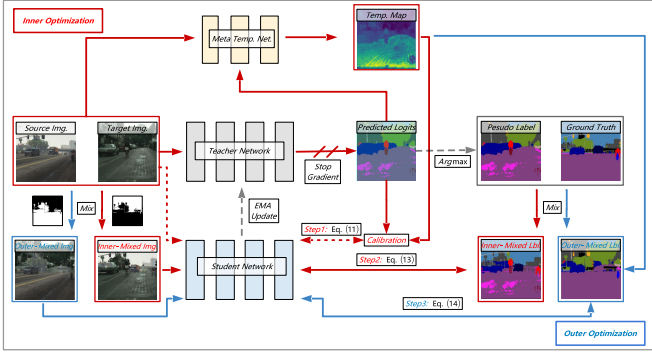


Fig. 2. **Pipeline illustration of DA-Cal.** Our framework consists of bi-level optimization: inner optimization (Steps 1-2) for calibrating predictions with Meta Temperature Network, and outer optimization (Step 3) for training the segmentation network with both calibrated soft and hard pseudo-labels. The supervised loss on source domain is omitted for clarity.

temperature map of the same spatial size, assigning a dedicated temperature  $\mathcal{T}_{ij}$  to each pixel:

$$p_{ij}^{\text{cal}} = \sigma_{\text{SM}}(f_{\theta}(x_{ij})/\mathcal{T}_{ij}). \quad (10)$$

This fine-grained calibration adapts to varying uncertainty levels across different regions, resulting in more accurate soft pseudo-labels. Notably, MTN is designed as a domain-shared module, leveraging source domain calibration knowledge to guide target domain calibration.

**Inner Optimization.** The inner optimization consists of two key steps:

**Step 1: Learning from Temperature-Calibrated Pseudo-Labels.** We first create a temporary copy  $\theta'$  of the student network parameters  $\theta$ . Then, we calibrate both source and target domain predictions using MTN. For both domains, we utilize calibrated soft pseudo-labels for training. A one-step gradient update of  $\theta'$  is performed based on these calibrated losses:

$$\theta'^{[k+1]} = \arg \min_{\theta'} \mathcal{L}_{\text{cal}}(S, T; \theta'^{[k]}, \psi^{[k]}), \quad (11)$$

which can be approximated as:

$$\theta'^{[k+1]} = \theta'^{[k]} - \alpha \nabla_{\theta'^{[k]}} \mathcal{L}_{\text{cal}}(S, T; \theta'^{[k]}, \psi^{[k]}), \quad (12)$$

where  $\psi$  represents the MTN parameters and  $\alpha$  is the inner-loop learning rate. Here,  $\mathcal{L}_{\text{cal}}$  is the calibrated cross-entropy loss based on soft pseudo-labels.

**Step 2: Updating MTN via Meta-Learning.** To evaluate the effectiveness of calibration, we test the updated network parameters  $\theta'^{[k+1]}$  on a specially constructed mixed dataset. This mixed dataset is created using ClassMix [44] technique, generating samples that are complementary to those used in the outer optimization to prevent self-reinforcement and overfitting. The performance on this mixed dataset reflects the network's domain adaptation capability. We compute the loss of  $\theta'^{[k+1]}$  on this mixed dataset and update the MTN parameters  $\psi$  through the meta-learning process:

$$\psi^{[k+1]} = \arg \min_{\psi^{[k]}} \mathcal{L}_{\text{mix}}(\theta'^{[k+1]}), \quad (13)$$

which is implemented as:

$$\psi^{[k+1]} = \psi^{[k]} - \beta \nabla_{\psi^{[k]}} \mathcal{L}_{\text{mix}}(\theta'^{[k]}) - \alpha \nabla_{\theta'^{[k]}} \mathcal{L}_{\text{cal}}(\theta'^{[k]}, \psi^{[k]}), \quad (14)$$

where  $\beta$  is the learning rate for MTN. The  $\mathcal{L}_{\text{mix}}$  is the cross-entropy loss computed on the mixed dataset, which combines source domain ground truth labels and target domain hard pseudo-labels. This mixed supervision provides a learning signal that helps evaluate how well the calibration improves the network's domain adaptation performance.

Since the MTN is domain-shared, calibration knowledge learned from the source domain (where ground truth is available) can gradually guide the calibration learning in the target domain.

**Outer Optimization.** After completing the inner optimization, we proceed with outer optimization to update the segmentation network parameters:

**Step 3: Updating the Segmentation Network.** The network is trained using the following total loss function:  $\mathcal{L}_{\text{total}} = \mathcal{L}^s + \hat{\mathcal{L}}^u$ , where  $\mathcal{L}^s$  is the supervised loss on the source domain computed with ground truth labels, and  $\hat{\mathcal{L}}^u$  is the unsupervised loss on the target domain. Unlike Eq. 2,  $\hat{\mathcal{L}}^u$  combines both hard and soft pseudo-label losses:

$$\hat{\mathcal{L}}^u = \frac{1}{N_T} \sum_{i=1}^{N_T} \frac{1}{HW} \sum_{j=1}^{H \times W} q(p_{ij}) (\ell_{ce}(f_{\theta}(x_{ij}^T), \hat{y}_{ij}^T) + \ell_{ce}(f_{\theta}(x_{ij}^T), p_{ij}^T, \text{cal})). \quad (15)$$

The calibrated soft pseudo-labels provide complementary supervision by preserving prediction uncertainty that hard labels discard. This framework not only achieves effective calibration but also brings additional segmentation performance gains by reducing confirmation bias in self-training. The algorithmic description is detailed in Alg. 1.

#### D. Practical Implementation

We offer two implementation strategies for our calibration approach: **DA-Cal-PH** and **DA-Cal-BI**, corresponding to post-hoc strategy and built-in strategy respectively.

**DA-Cal-PH (Post-Hoc).** In this implementation, MTN is used to calibrate network outputs during inference. Notably, MTN does not affect network accuracy, allowing it to be omitted when calibration is unnecessary. This provides flexibility for deployment in different application contexts.

**DA-Cal-BI (Built-In).** This implementation integrates calibration directly into the loss function by incorporating the MTN-predicted temperature  $\mathcal{T}$  into the cross-entropy loss:  $\ell_{ce}(x, y) = -\log(\sigma_{\text{SM}}(f_{\theta}(x) * \mathcal{T})^{(y)})/\mathcal{T}$ . Here, the network effectively learns a scoring function of the form  $g(x) = f(x) * \mathcal{T}$ . Consequently, since  $\arg \max_x f(x) = g(x)/\mathcal{T}$ , this formulation is analogous to post-hoc adjustment, enabling the network to produce calibrated outputs directly. The key advantage of DA-Cal-BI is that it produces a pre-calibrated network, eliminating the need for soft pseudo-labels in Eq. 13 and avoiding any additional inference overhead.

---

**Algorithm 1** Pseudo algorithms of DA-Cal.

---

- 1: **Inputs:** Source Domain  $D_S = (x_i^S, y_i^S)_{i=1}^{N_S}$ , Target Domain  $D_T = (x_i^T)_{i=1}^{N_T}$
  - 2: **Define:** Student Network  $f_\theta$ , Teacher Network  $g_\phi$ , Meta Temperature Network MTN  $h_\psi$ , Inner-loop Learning Rate  $\alpha$ , MTN Learning Rate  $\beta$ , Outer-loop Learning Rate  $\delta$ , EMA Coefficient  $\gamma$
  - 3: **Output:** Student Network  $f_\theta$
  - 4: **for** each batch of  $(x_i^S, y_i^S), x_i^T$  in  $D_S, D_T$  **do**
  - 5:    **# Inner Optimization:**
  - 6:    Create temporary copy  $\theta'^{[k]} \leftarrow \theta^{[k]}$  ▷ Step 1
  - 7:    Generate logits  $z_i^S = g_{\phi^{[k]}}(x_i^S), z_i^T = g_{\phi^{[k]}}(x_i^T)$
  - 8:    Predict temperatures  $\mathcal{T}_i^S = h_{\psi^{[k]}}([x_i^S, z_i^S]), \mathcal{T}_i^T = h_{\psi^{[k]}}([x_i^T, z_i^T])$
  - 9:    Calibrate predictions  $p_{i,cal}^S = \sigma_{SM}(z_i^S/\mathcal{T}_i^S), p_{i,cal}^T = \sigma_{SM}(z_i^T/\mathcal{T}_i^T)$
  - 10:    Update  $\theta'^{[k]}$  using gradient descent:  $\theta'^{[k+1]} \leftarrow \theta'^{[k]} - \alpha \nabla_{\theta'^{[k]}} \mathcal{L}_{cal}(S, T; \theta'^{[k]}, \psi^{[k]})$  by Eq. 12
  - 11:    Generate complementary mixed dataset ( [inner/outer-mixed image] ) using ClassMix ▷ Step 2
  - 12:    Update MTN parameters on [inner-mixed image]:  $\psi^{[k+1]} \leftarrow \psi^{[k]} - \beta \nabla_{\psi^{[k]}} \mathcal{L}_{mix}(\theta'^{[k+1]})$  by Eq. 14
  - 13:    **# Outer Optimization:**
  - 14:    Calculate supervised loss  $\mathcal{L}^S$  using ground truth labels  $y_i^S$  by Eq. 1
  - 15:    Generate target pseudo-labels  $\hat{y}_i^T = \operatorname{argmax}(g_\phi(x_i^T))$
  - 16:    Predict calibrated soft pseudo-labels  $p_{i,cal}^T = \sigma_{SM}(f_\theta(x_i^T)/h_{\psi^{[k+1]}}([x_i^T, f_\theta(x_i^T)]))$  ▷ Step 3
  - 17:    Calculate unsupervised loss  $\hat{\mathcal{L}}^u$  combining hard and soft pseudo-labels by Eq. 15
  - 18:    Update student network on both source image and [outer-mixed image]:  $\theta^{[k+1]} \leftarrow \theta^{[k]} - \delta \nabla_{\theta^{[k]}} (\mathcal{L}^S + \hat{\mathcal{L}}^u)$
  - 19:     $\phi^{[k+1]} \leftarrow \gamma \phi^{[k]} + (1 - \gamma) \theta^{[k+1]}$  ▷ EMA Update
  - 20: **end for**
- 

## IV. EXPERIMENTS

### A. Experimental Setup

**Datasets.** We evaluate our calibration approach on multiple benchmarks across two application domains where accurate uncertainty estimation is critical: autonomous driving and biomedical imaging. **For autonomous driving**, we consider both synthetic-to-real and clear-to-adverse weather domain adaptation scenarios. As synthetic datasets, we use GTAv [49], containing 24,966 images, and SYNTHIA [51], with 9,400 images. For real-world domains, we employ Cityscapes [11], which provides 2,975 training images and 500 validation images under clear weather conditions, and ACDC [52], which includes 1,600 training, 406 validation, and 2,000 test images captured under adverse weather conditions (fog, night, rain, and snow). **For biomedical imaging**, we evaluate on three widely used electron microscopy (EM) datasets exhibiting significant domain shifts. The VNC III dataset [18] contains 20 sections ( $1024 \times 1024$ ) of *Drosophila* brain tissue imaged using serial-section transmission electron microscopy (ssTEM). The Lucchi dataset [38] consists of two volumes ( $165 \times 1024 \times 768$ ) from mouse brain, acquired via focused ion beam scanning electron microscopy (FIB-SEM). The MitoEM dataset [62] comprises two large-scale volumes ( $1000 \times 4096 \times 4096$ ) from rat and human samples, imaged with multi-beam scanning electron microscopy (mbSEM).

**Evaluation Metrics.** For calibration quality, we consider three metrics: Expected Calibration Error (ECE) [21], Negative Log-Likelihood (NLL) [20], and Brier Score (BS) [4]. These metrics assess different aspects of prediction reliability and confidence alignment with actual accuracy. Note that different from classification task, semantic segmentation has a signifi-

cant class-pixel imbalance issue; therefore, we compute the above metrics from a class-pixel balanced perspective. For segmentation performance, we use mean Intersection over Union (mIoU) to evaluate the accuracy of semantic class predictions. Detailed descriptions of these metrics are provided in Appendix VI-A.

**UDA Methods.** For autonomous driving benchmarks, i.e., GTAv→Cityscapes, SYNTHIA→Cityscapes, and Cityscapes→ACDC, we adopt three baselines of increasing strength: DACS [58], DAFormer [25], and MIC [26]. DACS uses the DeepLabV2 [5] network based on ResNet-101 [23], while the latter two employ MiT-B5 [64] as the backbone. For biomedical imaging benchmarks, including VNC III→Lucchi (Subset1) and MitoEM-R→MitoEM-H, we adopt two baselines, DA-ISC [28] and SAFA [66], following the U-Net [50] structure.

**Calibration Baselines.** For a comprehensive comparison, we consider 4 calibration baselines, including the no calibration baseline (No Calib.), unsupervised calibration method (Ensemble [33], [40]), source-domain calibration (TempScale [21]), and cross-domain calibration (PseudoCal [27]) We also report metrics separately trained on source and target domains (NoAdapt/Oracle). Details of these implementation are provided in Appendix VI-B.

**Implementation Details.** We train all UDA methods using their official code. For Inner Optimization and MTN network, we adopt the SGD optimizer with a fixed learning rate of 0.01. For biomedical imaging benchmarks, we use CutMix [68] instead of ClassMix [44] since these are binary classification tasks. More training and implementation details are provided in Appendix VI-C.

TABLE I

CALIBRATION METRICS OF UDA ON AUTONOMOUS DRIVING SCENARIOS. NOTE THAT THESE METRICS ON SYN. ARE CALCULATED OVER 16 CLASSES.

Method	DACS [58]			DAFormer [25]			MIC [26]		
	ECE ( $\downarrow$ )	NLL ( $\downarrow$ )	BS ( $\downarrow$ )	ECE ( $\downarrow$ )	NLL ( $\downarrow$ )	BS ( $\downarrow$ )	ECE ( $\downarrow$ )	NLL ( $\downarrow$ )	BS ( $\downarrow$ )
<b>GTA5→Cityscapes</b>									
NoAdapt	0.2937	2.8097	0.8213	0.2098	1.7237	0.6262	0.1806	1.5172	0.6209
No Calib.	0.2289	1.7445	0.5701	0.1255	0.9084	0.3456	0.1042	0.7659	0.3034
Ensemble	0.1703	1.5054	0.5400	0.0914	0.7325	0.3212	0.0654	0.6971	0.2828
TempScal-src	0.1877	1.4393	0.5375	0.1030	0.8019	0.3325	0.0785	0.6682	0.2909
PseudoCal	0.1580	1.2893	0.5141	0.0818	0.7431	0.3242	0.0595	0.6242	0.2826
<b>DA-Cal (ours)</b>	<b>0.0965</b>	<b>0.8327</b>	<b>0.3279</b>	<b>0.0578</b>	<b>0.6332</b>	<b>0.2550</b>	<b>0.0459</b>	<b>0.5443</b>	<b>0.2116</b>
Oracle	0.0932	0.7626	0.3060	0.0632	0.5760	0.2314	0.0592	0.5390	0.2044
<b>SYNTHIA→Cityscapes</b>									
NoAdapt	0.3643	3.3656	0.8939	0.2705	2.4720	0.7061	0.2359	1.9054	0.5787
No Calib.	0.2730	2.3052	0.6516	0.1868	1.6878	0.4406	0.1668	1.2507	0.4763
Ensemble	0.2030	1.8273	0.5576	0.1449	1.3538	0.3935	0.1056	1.1054	0.3716
TempScal-src	0.2388	1.9255	0.6236	0.1658	1.4204	0.4234	0.1356	1.1332	0.4217
PseudoCal	0.2094	1.6939	0.6008	0.1447	1.2366	0.4108	0.1229	1.0870	0.4075
<b>DA-Cal (ours)</b>	<b>0.1530</b>	<b>1.2377</b>	<b>0.4652</b>	<b>0.0950</b>	<b>0.8155</b>	<b>0.3213</b>	<b>0.0822</b>	<b>0.8038</b>	<b>0.3256</b>
Oracle	0.0932	0.7626	0.3060	0.0632	0.5760	0.2314	0.0592	0.5390	0.2044
<b>Cityscapes→ACDC</b>									
NoAdapt	0.4431	4.7043	0.9792	0.3265	3.3191	0.7355	0.2584	2.7643	0.6267
No Calib.	0.3245	2.9316	0.7893	0.2282	1.9561	0.5350	0.1886	1.4702	0.4852
Ensemble	0.2565	2.3739	0.7326	0.1773	1.5063	0.4719	0.1456	1.2139	0.4234
TempScal-src	0.2807	2.4759	0.7529	0.2015	1.6227	0.5106	0.1567	1.3380	0.4569
PseudoCal	0.2375	2.1926	0.7221	0.1763	1.4173	0.4938	0.1463	1.2890	0.4416
<b>DA-Cal (ours)</b>	<b>0.1874</b>	<b>1.7141</b>	<b>0.5953</b>	<b>0.1216</b>	<b>1.0034</b>	<b>0.3732</b>	<b>0.1056</b>	<b>0.0913</b>	<b>0.3934</b>
Oracle	0.1842	1.5083	0.4738	0.1255	0.9948	0.3423	0.0884	0.7644	0.3167

TABLE II

CALIBRATION METRICS OF UDA ON ON BIOMEDICAL IMAGING SCENARIOS, WHICH ARE CALCULATED ONLY ON THE FOREGROUND.

Method	DA-ISC [28]			CAFA [66]		
	ECE	NLL	BS	ECE	NLL	BS
<b>VNC III → Lucchi (Subset1)</b>						
NoAdapt	0.3182	3.5611	0.6522	0.3182	3.5611	0.6522
No Calib.	0.2678	2.1510	0.5501	0.2167	2.0625	0.4445
Ensemble	0.1530	1.0610	0.4662	0.0869	0.7738	0.3544
TempScal-src	0.2011	0.8115	0.4726	0.1744	0.7489	0.3968
PseudoCal	0.1219	0.6202	0.4158	0.1086	0.5499	0.3531
<b>DA-Cal (ours)</b>	<b>0.0585</b>	<b>0.5770</b>	<b>0.3919</b>	<b>0.0520</b>	<b>0.5057</b>	<b>0.3321</b>
Oracle	0.0471	0.5023	0.3281	0.0471	0.5023	0.3281
<b>MitoEM-R → MitoEM-H</b>						
NoAdapt	0.2072	0.8347	0.6202	0.2072	0.8347	0.6202
No Calib.	0.1983	1.5984	0.4089	0.1404	1.3978	0.2897
Ensemble	0.0948	0.5371	0.3217	0.0710	0.5435	0.2557
TempScal-src	0.1385	0.6154	0.3531	0.1097	0.5101	0.2616
PseudoCal	0.0702	0.5049	0.3385	0.0689	0.4116	0.2475
<b>DA-Cal (ours)</b>	<b>0.0376</b>	<b>0.4835</b>	<b>0.3116</b>	<b>0.0325</b>	<b>0.3836</b>	<b>0.2324</b>
Oracle	0.0510	0.4019	0.2410	0.0510	0.4019	0.2410

## B. Results

**Calibration Performance.** DA-Cal significantly improves calibration across all benchmarks and UDA methods. In autonomous driving scenarios (Tab. I), our method reduces ECE from 10.42% to 4.59% with MIC on GTA5→Cityscapes—a 56% relative improvement—alongside substantial reductions in NLL (29%) and BS (30%). Similar improvements are observed for SYNTHIA→Cityscapes and Cityscapes→ACDC,

TABLE III

SEGMENTATION PERFORMANCE (mIoU) WITH DA-CAL. \* DENOTES THE REPRODUCED RESULT.

Method	baseline		w/ DA-Cal	
	GTA.→CS.	SYN.→CS.	GTA.→CS.	SYN.→CS.
DACS* [58]	51.9	<b>53.5</b>	47.9	<b>49.7</b>
DAFormer [25]	68.3	<b>69.4</b>	60.9	<b>62.2</b>
MIC* [26]	75.5	<b>76.3</b>	67.1	<b>68.0</b>
<b>VNC. → Lucchi</b> <b>Mito-R → Mito-H</b>				
DA-ISC [28]	68.7	<b>70.5</b>	74.8	<b>76.1</b>
CAFA [66]	71.8	<b>72.9</b>	76.3	<b>77.0</b>

where DA-Cal consistently outperforms all calibration baselines. These gains can be attributed to our pixel-wise MTN, which effectively captures spatial variations in prediction uncertainty, and the bi-level optimization framework, which facilitates more effective transfer of calibration knowledge from source to target domains.

In biomedical imaging scenarios (Tab. II), where domain shifts are more pronounced, DA-Cal achieves even greater improvements. For VNC III→Lucchi, our method reduces ECE from 21.67% to 5.20% with CAFA—a 76% reduction—with similarly strong results for MitoEM-R→MitoEM-H (77% ECE reduction). These results confirm the robustness of DA-Cal in scenarios with severe domain shifts.

**Segmentation Performance.** In addition to improving calibration, DA-Cal consistently enhances segmentation accuracy across all benchmarks (Tab. III). For autonomous driving, our method delivers steady mIoU gains over all baselines: 1.6%, 1.1%, and 0.8% improvements for DACS, DAFormer,

TABLE IV  
ANALYSIS OF DIFFERENT IMPLEMENTATION WITH DAFormer [25] ON  
GTAV  $\rightarrow$  CITYSCAPES.

$\mathcal{L}_{hard}$	$\mathcal{L}_{soft}$	DA-Cal-PH	DA-Cal-BI	mIoU ( $\uparrow$ )	ECE ( $\downarrow$ )
✓				68.3	0.1255
	✓			61.3	0.0857
		✓		67.5	0.0681
✓	✓			68.6	0.1048
✓		✓		<b>69.4</b>	<b>0.0578</b>
✓			✓	69.1	0.0603

and MIC on GTA5 $\rightarrow$ Cityscapes, with even larger gains on SYNTHIA $\rightarrow$ Cityscapes (1.8%, 1.3%, and 0.9%). In biomedical imaging, DA-Cal achieves notable performance boosts: 1.8% and 1.1% mIoU improvements for VNC III $\rightarrow$ Lucchi with DA-ISC and CAFA, and 1.3% and 0.7% for MitoEM-R $\rightarrow$ MitoEM-H. These consistent improvements demonstrate that integrating both hard and calibrated soft pseudo-labels into the unsupervised loss preserves valuable uncertainty information that would otherwise be discarded, effectively reducing confirmation bias in self-training. By simultaneously improving both calibration and segmentation performance, DA-Cal highlights the intrinsic connection between reliable confidence estimation and accurate semantic prediction in domain adaptation.

### C. Ablation Study and Discussion

Additional analyses can be found in Appendix VI-D-VI-H. **Analysis of Implementation.** Tab. IV compares different implementation strategies on DAFormer [25]. From a theoretical perspective (Sec. III-B), perfectly calibrated soft pseudo-labels are equivalent to hard labels in expectation, as they reflect the true class likelihoods. Intuitively, soft labels act as a weighted average over all possible classes, and when properly calibrated, they provide the same expected supervision as stochastic sampling from hard labels. Empirically, however, we observe that uncalibrated soft labels significantly degrade segmentation performance, even though they yield better calibration. For instance, replacing hard labels with soft ones (Row 2) causes a 7.0% drop in mIoU, despite a 0.0398 improvement in ECE. This highlights that while soft labels are theoretically sound, their effectiveness in practice is heavily dependent on calibration quality. In Row 3, we isolate the effect of using only calibrated soft labels with our DA-Cal-PH variant. Although calibration improves (ECE drops to 0.0681), segmentation performance (67.5% mIoU) still lags behind the hard-label baseline (68.3% mIoU). This suggests that, even when calibrated, soft labels alone offer less stable supervision, particularly in early training when model confidence is unreliable. In contrast, hard labels—despite introducing confirmation bias—provide clearer and more consistent learning signals. When combining both types of labels (Row 4), we observe modest improvements in both segmentation (+0.3% mIoU) and calibration (-0.0207 ECE), highlighting the complementary effect of these supervision signals. The introduction of our DA-Cal framework (Row 5/6) delivers substantial improvements. With DA-Cal-PH, we achieve a

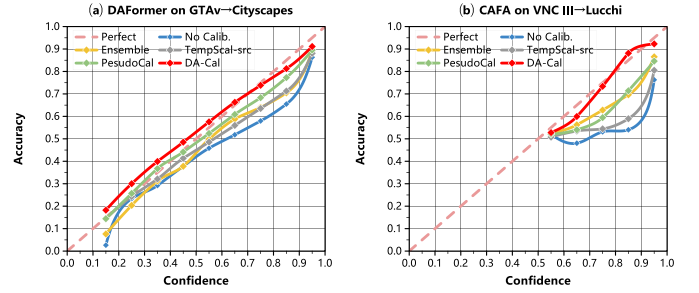


Fig. 3. Comparison of DA-Cal and Baseline Methods on Reliability Diagrams.

remarkable calibration improvement (0.0677 ECE reduction) alongside a significant segmentation performance gain (+1.1% mIoU). Similarly, DA-Cal-BI yields comparable improvements (0.0652 ECE reduction and +0.8% mIoU gain), with the added benefit of introducing no additional inference overhead. These results demonstrate that well-calibrated soft pseudo-labels not only improve confidence estimation but also enhance segmentation accuracy by providing more reliable supervision signals during domain adaptation.

**Qualitative Comparisons.** Fig. 3 clearly demonstrates our method’s superior calibration performance compared to baseline approaches. The reliability diagrams show that our approach nearly perfectly aligns with the ideal diagonal line (representing perfect calibration), with minimal gaps between predicted confidence and actual accuracy across all confidence bins. While other methods exhibit significant calibration errors, our method achieves remarkable calibration precision, resulting in confidence scores that accurately reflect true prediction reliability in cross-domain settings.

**Discussion on Temperature Scaling.** Fig. 4 demonstrates the relationship between calibration performance and temperature values across different methods. We observe that source and target domains exhibit notably different optimal temperature parameters—a challenge further amplified in domain adaptation settings. This discrepancy means that temperatures optimized on source data (TempScal-src) yield suboptimal calibration when applied to target domains. While PseudoCal [27] attempts to address this through pseudo-target synthesis, its sample-level approach is ill-suited for the pixel-level nature of segmentation tasks. Furthermore, conventional temperature scaling applies a global parameter without considering the crucial spatial context in segmentation. Our DA-Cal method (red line) maintains superior calibration across all temperature values and network architectures by explicitly modeling target domain calibration with spatial awareness. It also eliminates the need for temperature parameter tuning, offering a robust solution when target domain labels are unavailable for calibration optimization.

**Visualization of Temperature Maps.** Fig. 5 illustrates the learned temperature maps across various domain adaptation benchmarks. These visualizations highlight how DA-Cal adaptively calibrates model confidence in a spatially-aware manner. The temperature maps serve a dual purpose: they sharpen logit distributions in regions with reliable predictions (indicated by lower  $\mathcal{T}$  values and darker colors), while smoothing distri-

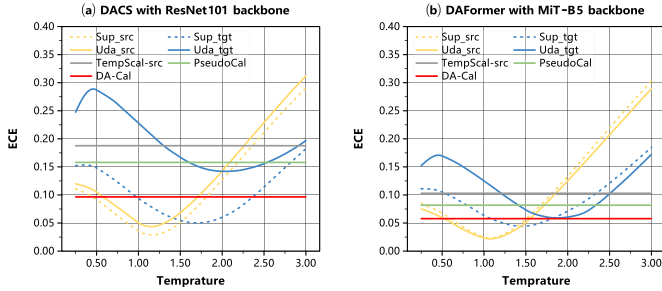


Fig. 4. Ablation study on temperature scaling for GTA.  $\rightarrow$ CS. benchmark across different methods.

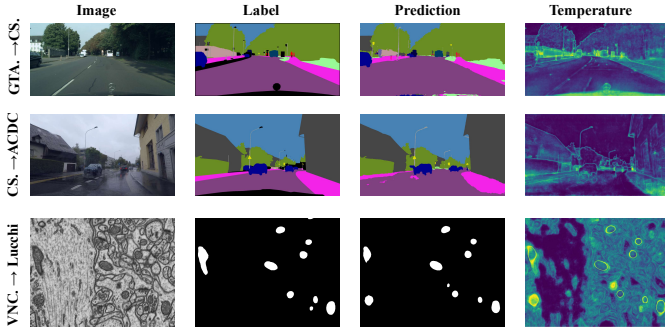


Fig. 5. Visualization of temperature maps on different benchmarks.

contributions in potentially erroneous areas (higher  $\mathcal{T}$  values with lighter colors). This spatial adaptability is especially beneficial for semantic segmentation, where prediction confidence can vary significantly across different image regions. Lower temperatures help preserve confident predictions in reliable areas, whereas higher temperatures suppress overconfident yet incorrect predictions in uncertain regions. This dynamic calibration approach greatly improves the model’s reliability across diverse domain adaptation scenarios.

## V. CONCLUSION

In this work, we present DA-Cal, a novel cross-domain calibration framework designed for unsupervised domain adaptation (UDA) in semantic segmentation. Our method reformulates the target domain calibration challenge as an optimization problem over soft pseudo-labels, leveraging a bi-level optimization strategy inspired by meta-learning. At its core, DA-Cal introduces the Meta Temperature Network (MTN), which enables pixel-wise adaptive temperature scaling, effectively reducing calibration errors that hinder UDA performance. To further boost generalization and prevent overfitting, we incorporate complementary domain-mixing strategies. DA-Cal integrates seamlessly into existing self-training UDA frameworks, offering improved calibration quality and enhanced segmentation accuracy—all without introducing additional inference overhead. Extensive experiments on multiple benchmarks demonstrate the effectiveness of our approach, establishing a new standard for reliable and well-calibrated cross-domain semantic segmentation.

## VI. APPENDIX

This appendix provides additional details and analyses to complement our main paper. We include in-depth explanations of our evaluation metrics, implementation details, ablation studies, and additional visualization results. Specifically, the appendix is organized as follows:

- **Section VI-A** introduces the calibration metrics used in our evaluation, including Expected Calibration Error (ECE), Negative Log-Likelihood (NLL), and Brier Score (BS). We also describe how these metrics are adapted for semantic segmentation.
- **Section VI-B** provides details on the baseline calibration methods used for comparison.
- **Section VI-C** describes additional implementation details of DA-Cal, including the design of the Meta Temperature Network (MTN) and optimization strategies.
- **Section VI-D** presents an analysis of training strategies, demonstrating the effectiveness of EMA-based MTN updates and warm-up calibration.
- **Section VI-E** explores the impact of DA-Cal’s hyperparameters on performance.
- **Section VI-F** evaluates the computational efficiency of DA-Cal in terms of GPU memory and training time.
- **Section VI-G** studies the effect of different domain-mixing strategies on segmentation and calibration performance.
- **Section VI-H** showcases additional visualization results to further illustrate the effectiveness of DA-Cal.

### A. Introduction of Calibration Metrics

In this section, we introduce the calibration metrics used in our evaluation, including Expected Calibration Error (ECE), Negative Log-Likelihood (NLL), and Brier Score (BS).

**Expected Calibration Error (ECE)** [21] measures the difference between the predicted confidence and the actual accuracy. It is computed by partitioning predictions into multiple bins and calculating the weighted average of absolute differences between confidence and accuracy in each bin. The formula is defined as:

$$\text{ECE} = \sum_{m=1}^M \frac{|B_m|}{N} |\text{acc}(B_m) - \text{conf}(B_m)|, \quad (16)$$

where  $M$  is the number of bins,  $B_m$  denotes the set of predictions that fall into the  $m$ -th bin,  $|B_m|$  is the number of samples in that bin,  $N$  is the total number of samples,  $\text{acc}(B_m)$  is the average accuracy of samples in bin  $m$ , and  $\text{conf}(B_m)$  is the average confidence.

**Negative Log-Likelihood (NLL)** [20] is a well-known metric for assessing probabilistic predictions, which is also known as the cross-entropy loss. It evaluates how well a model assigns probabilities to the correct labels, with lower values indicating better calibration. The NLL is defined as:

$$\text{NLL} = -\frac{1}{N} \sum_{i=1}^N \sum_{c=1}^C y_{i,c} \log p_{i,c}, \quad (17)$$

where  $N$  is the total number of pixels,  $C$  is the number of classes,  $y_{i,c}$  is the one-hot encoded ground-truth label

indicating whether pixel  $i$  belongs to class  $c$ , and  $p_{i,c}$  is the predicted probability for class  $c$ .

**Brier Score (BS)** [4] quantifies the mean squared error between predicted probabilities and the actual one-hot encoded labels. It captures both calibration and sharpness aspects of the predictions. The BS is defined as:

$$\text{BS} = \frac{1}{N} \sum_{i=1}^N \sum_{c=1}^C (p_{i,c} - y_{i,c})^2. \quad (18)$$

Unlike classification tasks, where these metrics are computed on a sample basis, semantic segmentation involves per-pixel evaluation, leading to severe class imbalance issues. To address this, we compute ECE, NLL, and BS at the class level and then take an average across all classes:

$$\mathcal{M}_{\text{class}} = \frac{1}{C} \sum_{c=1}^C \mathcal{M}(c), \quad (19)$$

where  $\mathcal{M}$  represents any of the above metrics (ECE, NLL, or BS) computed for class  $c$ .

To improve computational efficiency, we sample 10,000 pixels per image to estimate these metrics following [13].

### B. Details of Calibration Baselines

We compare DA-Cal with several existing calibration methods:

**Ensemble** [33], [40]: We train each segmentation model three times with different random seeds. During inference, we average the predicted logits from these models before applying softmax to obtain final calibrated probabilities.

**TempScal-src** [21]: This method applies temperature scaling using a hold-out validation set from the source domain to find the optimal temperature  $\mathcal{T}$  to minimize NLL. The calibrated probabilities are computed as:

$$p_{\text{cal}} = \text{softmax}(z/\mathcal{T}), \quad (20)$$

where  $z$  represents the pre-softmax logits.

**PseudoCal** [27]: This method synthesizes pseudo-target samples using a mixup [70] strategy. The synthesized samples are used to learn temperature scaling parameters in the target domain. Unlike classification-based approaches that model samples independently, we apply PseudoCal at the pixel level.

**NoAdapt/Oracle**: The NoAdapt baseline trains models only on the source domain and directly evaluates them on the target domain. The Oracle model, on the other hand, is trained with labels from the target domain, providing an well-calibrated baseline for calibration performance.

### C. More Implementation Details of DA-Cal

**EMA Update and Warm-up Strategy**: The Meta Temperature Network (MTN) parameters are updated using an Exponential Moving Average (EMA) strategy. EMA ensures stable updates by gradually incorporating new knowledge while retaining past information. Since MTN progressively enhances calibration performance, we introduce a warm-up

TABLE V  
IMPACT OF EMA UPDATES AND WARM-UP CALIBRATION ON DA-CAL PERFORMANCE.

Base	EMA(MTN)	Warm-up ( $\lambda_{\text{soft}}$ )	mIoU (%) $\uparrow$	ECE $\downarrow$
✓	-	-	68.3	0.1255
-	-	-	68.7	0.0687
-	✓	-	68.9	0.0591
-	-	✓	69.2	0.0633
-	✓	✓	<b>69.4</b>	<b>0.0578</b>

strategy to gradually increase the weight of soft pseudo-label supervision:

$$\lambda_{\text{soft}} = \min\left(1, \frac{t}{T_{\text{warm-up}}}\right), \quad (21)$$

where  $t$  is the current training iteration, and  $T_{\text{warm-up}}$  is the total number of warm-up iterations, which we set to half of the total training iterations. A detailed analysis of the effectiveness of the EMA update and warm-up strategy is provided in Section VI-D.

**MTN Architecture**: The MTN is designed as a lightweight calibration module to minimize computational overhead. It consists of a stack of convolutional layers followed by Batch-Norm and ReLU activation. To balance model complexity and performance, we adopt a three-layer architecture in our experiments. A comprehensive analysis of the trade-off between MTN capacity and performance is provided in Section VI-E.

**Efficient Inner Optimization**: To improve computational efficiency, we optimize only the segmentation head while keeping the backbone frozen during inner-loop updates. This significantly reduces the memory footprint and accelerates training. The high-order meta-loss is computed solely for the segmentation head parameters, ensuring efficient parameter updates. A detailed evaluation of the computational overhead introduced by DA-Cal, including GPU memory usage and training time, is presented in Section VI-F

### D. Training Strategies Analysis of DA-Cal

We evaluate the effectiveness of EMA-based MTN updates and warm-up calibration for soft pseudo-labels on the DAFormer [25] using the GTA<sub>v</sub>→Cityscapes benchmark. Table V reports the impact of these strategies on segmentation and calibration performance.

**Effect of Warm-up Strategy on Segmentation Performance**. From Table V, we observe that applying the warm-up strategy ( $\lambda_{\text{soft}}$ ) significantly improves the segmentation performance (mIoU). Specifically, compared to the baseline without warm-up (row 2 vs. row 4), mIoU increases from 68.7% to 69.2%, demonstrating a clear benefit. This improvement can be attributed to the gradual introduction of soft pseudo-label supervision, which prevents early-stage noisy pseudo-labels from negatively affecting model training. By progressively increasing the weight of soft pseudo-labels, the network learns more reliable supervision signals, thereby enhancing segmentation accuracy.

**Effect of EMA-based MTN Updates on Calibration Performance**. The results also indicate that the EMA-based

TABLE VI  
HYPERPARAMETER SENSITIVITY ANALYSIS FOR DA-CAL.

MTN layers	1	2	3	4
mIoU (%) $\uparrow$	68.9	69.4	<b>69.4</b>	69.3
ECE $\downarrow$	0.0672	0.0610	0.0578	<b>0.0569</b>
Inner LR	0.1	0.05	0.01	0.001
mIoU (%) $\uparrow$	68.7	69.4	<b>69.4</b>	69.1
ECE $\downarrow$	0.0710	0.0593	<b>0.0578</b>	0.0649

MTN updates primarily contribute to improving calibration performance. When enabling EMA (row 2 vs. row 3), the Expected Calibration Error (ECE) decreases from 0.0687 to 0.0591, showing that the EMA strategy effectively stabilizes temperature updates, leading to better calibration. This is because EMA ensures smoother updates to the MTN parameters, preventing abrupt fluctuations and improving the consistency of pixel-wise temperature scaling.

Furthermore, combining EMA with the warm-up strategy (row 5) achieves the best overall performance, with mIoU = 69.4% and ECE = 0.0578. This confirms that while warm-up enhances segmentation accuracy, EMA plays a crucial role in refining the calibration quality.

#### E. Hyper-parameters Analysis

The key hyperparameters of DA-Cal include the number of layers in MTN, the learning rate for inner optimization, and the learning rate for MTN. We use SGD with a learning rate of 0.01 for both inner optimization and MTN training. Table VI explores the impact of these hyperparameters with DAFormer [25] using the GTA $\rightarrow$ Cityscapes benchmark.

**Impact of MTN Depth on Performance.** From Table VI, we observe that increasing the number of MTN layers from 1 to 3 improves both segmentation (mIoU) and calibration (ECE). Further increasing to 4 layers does not yield additional benefits. This suggests diminishing returns for deeper MTN architectures. Based on these observations, we adopt a 3-layer MTN in our final model to balance calibration effectiveness and computational efficiency.

**Impact of Inner Learning Rate on Performance.** For the inner optimization learning rate, we find that a learning rate of 0.01 yields the best results, while a higher learning rate (0.1) leads to degraded calibration performance (ECE = 0.0710), likely due to instability in meta-updates, and a lower learning rate (0.001) results in worse calibration (ECE = 0.0649) and slightly lower segmentation performance (69.1% mIoU), suggesting slower convergence.

#### F. DA-Cal Efficiency Analysis

Our method is computationally efficient. Table VII compares GPU memory usage and training time for DAFormer [25] and DACS [58] with and without DA-Cal.

**Computational Overhead Analysis.** From Table VII, we observe that integrating DA-Cal introduces additional computational cost but remains practical. Specifically, for DAFormer, DA-Cal increases GPU memory usage from 9,807 MB to

TABLE VII  
COMPARISON OF GPU MEMORY AND TRAINING TIME.

Method	GPU Memory (MB)	Training Time (h)
DAFormer	9,807	16.2
w/ DA-Cal	13,409	22.5
DACS	11,078	25.4
w/ DA-Cal	14,485	31.9

TABLE VIII  
COMPARISON OF MIXING STRATEGIES WITH DAFORMER ON GTA  $\rightarrow$  CS. AND CAFA ON VNC.  $\rightarrow$  LUCCHI.

Mixing Strategy		GTA $\rightarrow$ CS. VNC. $\rightarrow$ Lucchi			
		mIoU $\uparrow$ ECE $\downarrow$		mIoU $\uparrow$ ECE $\downarrow$	
Baseline	-	68.3	0.2289	71.8	0.2167
ClassMix	Same	69.0	0.0638	72.0	0.0785
	Random	69.3	0.0612	72.0	0.0774
	<b>Complementary</b>	<b>69.4</b>	<b>0.0578</b>	72.1	0.0705
CutMix	Same	68.9	0.0641	72.6	0.0596
	Random	68.9	0.0607	72.9	0.0563
	<b>Complementary</b>	69.2	0.0591	<b>72.9</b>	<b>0.0520</b>

13,409 MB (+36.7%) and training time from 16.2 hours to 22.5 hours (+38.9%). Similarly, for DACS, DA-Cal increases GPU memory from 11,078 MB to 14,485 MB (+30.7%) and training time from 25.4 hours to 31.9 hours (+25.6%).

**Efficiency-Performance Trade-off.** Although DA-Cal introduces moderate overhead, the significant improvements in both segmentation accuracy and calibration quality (ECE) justify the additional cost. The increase in memory usage is mainly due to the meta-learning framework, which requires storing temporary network states for gradient computation. However, the efficient inner-loop optimization (Section VI-C) mitigates excessive computational burden by freezing the backbone, ensuring that the extra cost remains manageable.

#### G. Ablation on Mixing Strategies

ClassMix [44] is used in our autonomous driving benchmarks, ensuring inner and outer optimization use complementary masks to avoid self-reinforcement and overfitting. Specifically, ClassMix randomly selects half of the source domain classes for mixing in each iteration. To enforce complementary learning, we assign the remaining half of the classes to the inner optimization, ensuring that the two optimization stages utilize disjoint class masks. This prevents the model from overfitting to a fixed subset of samples and improves generalization.

**Analysis of Mixing Strategies.** Table VIII compares different mixing strategies. Using the same mask for both inner and outer optimization results in slightly lower performance (69.0% mIoU, 0.0638 ECE), likely due to self-reinforcement effects where the model overfits to specific regions. Randomly selecting masks per iteration improves results (69.3% mIoU, 0.0612 ECE), but lacks structured control over the mixed regions. Our complementary mask strategy further enhances

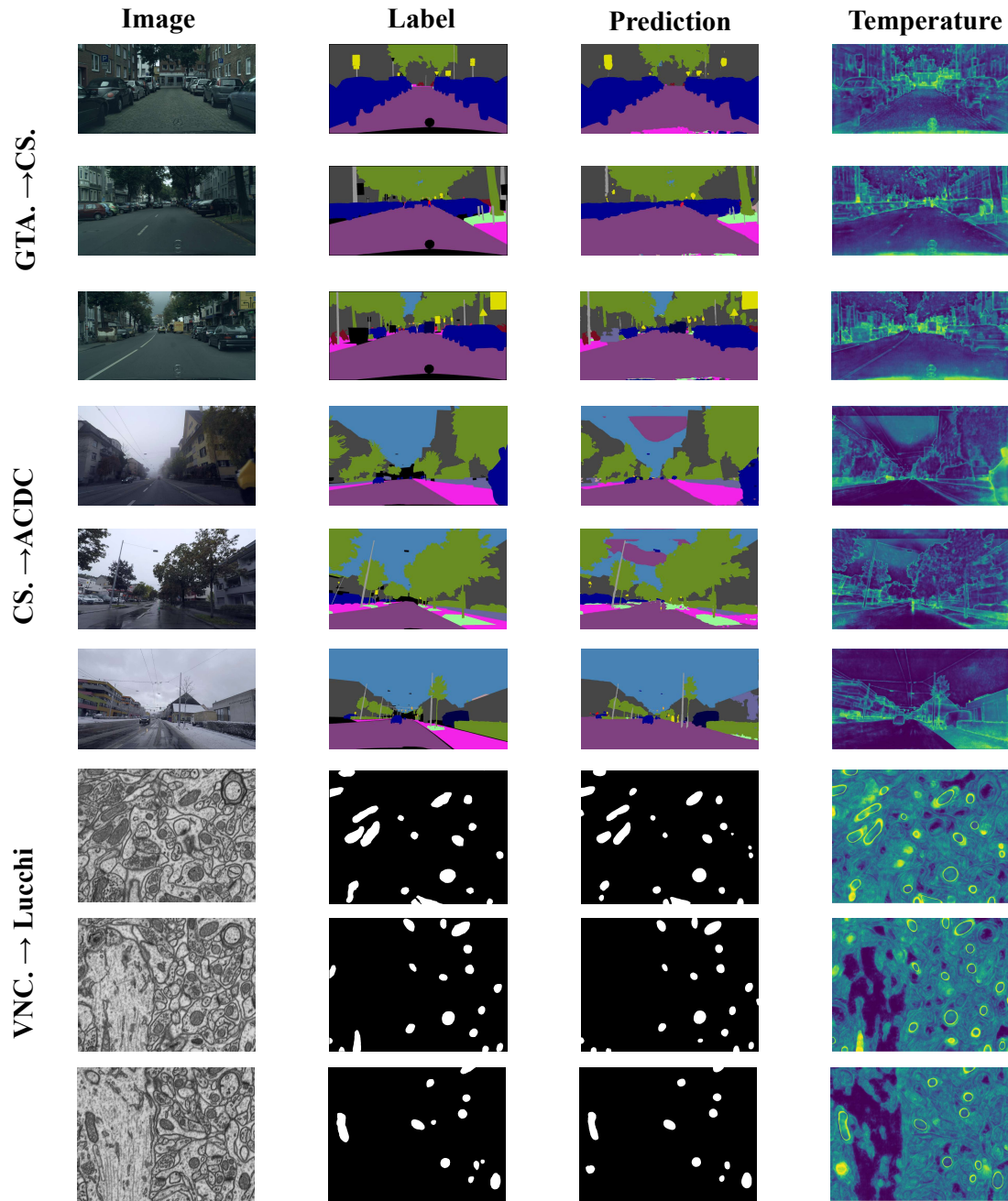


Fig. 6. Visualization of learned temperature maps on different adaptation benchmarks: GTA.  $\rightarrow$  CS. (synthetic-to-real), CS.  $\rightarrow$  ACDC (clear-to-adverse weather), and VNC.  $\rightarrow$  Lucchi (biomedical segmentation).

performance (69.4% mIoU, 0.0578 ECE) by ensuring that inner and outer optimization operate on disjoint class sets, leading to better generalization and calibration.

**Region-Level CutMix for Biomedical Imaging.** For biomedical imaging, we adopt region-level CutMix [68], which is more suitable for foreground segmentation tasks such as binary tissue segmentation. In binary settings like VNC  $\rightarrow$  Lucchi, ClassMix becomes less effective due to the lack of class diversity. Specifically, ClassMix may remove all foreground regions during mixing, resulting in poor supervision signals. Unlike ClassMix, which relies on class-wise separation and assumes multiple semantic categories, CutMix operates at

the region level, directly mixing local patches from different images. This region-aware augmentation is particularly beneficial for binary tasks where the goal is to distinguish foreground structures from background. To validate this, we compare the two strategies on this benchmark. As shown in Table VIII, CutMix outperforms ClassMix, achieving a higher IoU (72.9% vs. 72.1%) and a lower expected calibration error (ECE: 0.0520 vs. 0.0704). These results highlight the importance of selecting augmentation strategies that align with the dataset characteristics—region-aware mixing proves essential for effective biomedical domain adaptation.

## H. More Visualization Results

To further validate DA-Cal’s effectiveness, we provide additional temperature map visualizations across various domain adaptation tasks. Figure 6 showcases results for synthetic-to-real adaptation (GTA.  $\rightarrow$  CS.), clear-to-adverse weather adaptation (CS.  $\rightarrow$  ACDC), and biomedical segmentation (VNC.  $\rightarrow$  Lucchi). These results highlight how DA-Cal dynamically adjusts temperature values to enhance model calibration, particularly in regions prone to miscalibration.

**Synthetic-to-Real Adaptation (GTA.  $\rightarrow$  CS.).** For synthetic-to-real adaptation, we observe that regions affected by domain shifts, such as road textures, building facades, and vegetation, exhibit higher temperatures. This suggests that DA-Cal effectively identifies areas where synthetic textures differ from real-world counterparts, thereby reducing overconfidence in these regions. Moreover, object boundaries (e.g., vehicles, poles, pedestrians) tend to have elevated temperatures, preventing the model from being overly confident in ambiguous regions.

**Clear-to-Adverse Weather Adaptation (CS.  $\rightarrow$  ACDC).** When adapting from clear-weather Cityscapes to the adverse-weather ACDC dataset, the temperature maps reveal higher uncertainty in regions affected by fog, snow, and rain. Road areas remain well-calibrated (low temperatures), while occluded objects and distant structures show elevated temperatures. This demonstrates that DA-Cal effectively captures visibility degradation, ensuring better calibration in uncertain regions.

**Biomedical Segmentation (VNC III  $\rightarrow$  Lucchi).** In biomedical domain adaptation, the temperature maps exhibit greater adjustments around cellular boundaries, reflecting the inherent segmentation ambiguity in these regions. Unlike urban scenes—where uncertainty primarily arises from domain shifts—uncertainty here stems from the challenge of distinguishing fine-grained structures from background tissue. This suggests that DA-Cal enhances model reliability in complex foreground-background segmentation tasks, successfully adapting to the unique characteristics of biomedical imagery.

## REFERENCES

- [1] Araslanov, N., Roth, S.: Self-supervised augmentation consistency for adapting semantic segmentation. In: Proceedings of the IEEE/CVF Conference on Computer Vision and Pattern Recognition. pp. 15384–15394 (2021)
- [2] Bhojanapalli, S., Chakrabarti, A., Glasner, D., Li, D., Unterthiner, T., Veit, A.: Understanding robustness of transformers for image classification. In: Proceedings of the IEEE/CVF international conference on computer vision. pp. 10231–10241 (2021)
- [3] Bojarski, M., Del Testa, D., Dworakowski, D., Firner, B., Flepp, B., Goyal, P., Jackel, L.D., Monfort, M., Muller, U., Zhang, J., et al.: End to end learning for self-driving cars. arXiv preprint arXiv:1604.07316 (2016)
- [4] Brier, G.W.: Verification of forecasts expressed in terms of probability. Monthly weather review **78**(1), 1–3 (1950)
- [5] Chen, L.C., Papandreou, G., Kokkinos, I., Murphy, K., Yuille, A.L.: Deeplab: Semantic image segmentation with deep convolutional nets, atrous convolution, and fully connected crfs. IEEE transactions on pattern analysis and machine intelligence **40**(4), 834–848 (2017)
- [6] Chen, L.C., Papandreou, G., Schroff, F., Adam, H.: Rethinking atrous convolution for semantic image segmentation. arXiv preprint arXiv:1706.05587 (2017)
- [7] Chen, M., Xue, H., Cai, D.: Domain adaptation for semantic segmentation with maximum squares loss. In: Proceedings of the IEEE/CVF International Conference on Computer Vision. pp. 2090–2099 (2019)
- [8] Chen, Y., Li, W., Van Gool, L.: Road: Reality oriented adaptation for semantic segmentation of urban scenes. In: Proceedings of the IEEE conference on computer vision and pattern recognition. pp. 7892–7901 (2018)
- [9] Cheng, B., Misra, I., Schwing, A.G., Kirillov, A., Girdhar, R.: Masked-attention mask transformer for universal image segmentation. In: Proceedings of the IEEE/CVF conference on computer vision and pattern recognition. pp. 1290–1299 (2022)
- [10] Cheng, B., Schwing, A., Kirillov, A.: Per-pixel classification is not all you need for semantic segmentation. Advances in Neural Information Processing Systems **34**, 17864–17875 (2021)
- [11] Cordts, M., Omran, M., Ramos, S., Rehfeld, T., Enzweiler, M., Benenson, R., Franke, U., Roth, S., Schiele, B.: The cityscapes dataset for semantic urban scene understanding. In: Proceedings of the IEEE conference on computer vision and pattern recognition. pp. 3213–3223 (2016)
- [12] Cortes, C., Mohri, M., Riley, M., Rostamizadeh, A.: Sample selection bias correction theory. In: International conference on algorithmic learning theory. pp. 38–53. Springer (2008)
- [13] De Jorge, P., Volpi, R., Torr, P.H., Rogez, G.: Reliability in semantic segmentation: Are we on the right track? In: Proceedings of the IEEE/CVF Conference on Computer Vision and Pattern Recognition. pp. 7173–7182 (2023)
- [14] Ding, Z., Han, X., Liu, P., Niethammer, M.: Local temperature scaling for probability calibration. In: Proceedings of the IEEE/CVF International Conference on Computer Vision. pp. 6889–6899 (2021)
- [15] Esteva, A., Kuprel, B., Novoa, R.A., Ko, J., Swetter, S.M., Blau, H.M., Thrun, S.: Dermatologist-level classification of skin cancer with deep neural networks. nature **542**(7639), 115–118 (2017)
- [16] Finn, C., Abbeel, P., Levine, S.: Model-agnostic meta-learning for fast adaptation of deep networks. In: International conference on machine learning. pp. 1126–1135. PMLR (2017)
- [17] Ganin, Y., Lempitsky, V.: Unsupervised domain adaptation by backpropagation. In: International conference on machine learning. pp. 1180–1189. PMLR (2015)
- [18] Gerhard, S., Funke, J., Martel, J., Cardona, A., Fetter, R.: Segmented anisotropic sstem dataset of neural tissue. figshare pp. 0–0 (2013)
- [19] Gong, Y., Lin, X., Yao, Y., Dieterich, T.G., Divakaran, A., Gervasio, M.: Confidence calibration for domain generalization under covariate shift. In: Proceedings of the IEEE/CVF international conference on computer vision. pp. 8958–8967 (2021)
- [20] Goodfellow, I., Bengio, Y., Courville, A., Bengio, Y.: Deep learning, vol. 1. MIT press Cambridge (2016)
- [21] Guo, C., Pleiss, G., Sun, Y., Weinberger, K.Q.: On calibration of modern neural networks. In: International conference on machine learning. pp. 1321–1330. PMLR (2017)
- [22] He, H., Bai, Y., Garcia, E.A., Li, S.: Adasyn: Adaptive synthetic sampling approach for imbalanced learning. In: 2008 IEEE international joint conference on neural networks (IEEE world congress on computational intelligence). pp. 1322–1328. Ieee (2008)
- [23] He, K., Zhang, X., Ren, S., Sun, J.: Deep residual learning for image recognition. In: Proceedings of the IEEE conference on computer vision and pattern recognition. pp. 770–778 (2016)
- [24] He, L., Todorovic, S.: Attention decomposition for cross-domain semantic segmentation. In: European Conference on Computer Vision. pp. 414–431. Springer (2025)
- [25] Hoyer, L., Dai, D., Van Gool, L.: Daformer: Improving network architectures and training strategies for domain-adaptive semantic segmentation. In: Proceedings of the IEEE/CVF Conference on Computer Vision and Pattern Recognition. pp. 9924–9935 (2022)
- [26] Hoyer, L., Dai, D., Wang, H., Van Gool, L.: Mic: Masked image consistency for context-enhanced domain adaptation. In: Proceedings of the IEEE/CVF Conference on Computer Vision and Pattern Recognition. pp. 11721–11732 (2023)
- [27] Hu, D., Liang, J., Wang, X., Foo, C.S.: Pseudo-calibration: improving predictive uncertainty estimation in unsupervised domain adaptation. In: Forty-first International Conference on Machine Learning (2024)
- [28] Huang, W., Liu, X., Cheng, Z., Zhang, Y., Xiong, Z.: Domain adaptive mitochondria segmentation via enforcing inter-section consistency. In: International Conference on Medical Image Computing and Computer-Assisted Intervention. pp. 89–98. Springer (2022)
- [29] Huo, X., Xie, L., Zhou, W., Li, H., Tian, Q.: Focus on your target: A dual teacher-student framework for domain-adaptive semantic segmentation. arXiv preprint arXiv:2303.09083 (2023)
- [30] Ji, B., Jung, H., Yoon, J., Kim, K., et al.: Bin-wise temperature scaling (bts): improvement in confidence calibration performance through sim-

- ple scaling techniques. In: 2019 IEEE/CVF International Conference on Computer Vision Workshop (ICCVW). pp. 4190–4196. IEEE (2019)
- [31] Jiang, X., Osl, M., Kim, J., Ohno-Machado, L.: Calibrating predictive model estimates to support personalized medicine. *Journal of the American Medical Informatics Association* **19**(2), 263–274 (2012)
- [32] Kassapis, E., Dikov, G., Gupta, D.K., Nugteren, C.: Calibrated adversarial refinement for stochastic semantic segmentation. In: Proceedings of the IEEE/CVF International Conference on Computer Vision. pp. 7057–7067 (2021)
- [33] Lakshminarayanan, B., Pritzel, A., Blundell, C.: Simple and scalable predictive uncertainty estimation using deep ensembles. *Advances in neural information processing systems* **30** (2017)
- [34] Lee, D.H., et al.: Pseudo-label: The simple and efficient semi-supervised learning method for deep neural networks. In: Workshop on challenges in representation learning, ICML. vol. 3, p. 896. Atlanta (2013)
- [35] Li, W., Sun, R., Zhang, T.: A universal degradation-based bridging technique for domain adaptive semantic segmentation. *arXiv preprint arXiv:2412.10339* (2024)
- [36] Liu, H., Simonyan, K., Yang, Y.: Darts: Differentiable architecture search. *arXiv preprint arXiv:1806.09055* (2018)
- [37] Long, J., Shelhamer, E., Darrell, T.: Fully convolutional networks for semantic segmentation. In: Proceedings of the IEEE conference on computer vision and pattern recognition. pp. 3431–3440 (2015)
- [38] Lucchi, A., Li, Y., Fua, P.: Learning for structured prediction using approximate subgradient descent with working sets. In: Proceedings of the IEEE Conference on Computer Vision and Pattern Recognition. pp. 1987–1994 (2013)
- [39] Mata, C., Ranasinghe, K., Ryoo, M.S.: Copt: Unsupervised domain adaptive segmentation using domain-agnostic text embeddings. In: European Conference on Computer Vision. pp. 424–440. Springer (2025)
- [40] Mehrtash, A., Wells, W.M., Tempny, C.M., Abolmaesumi, P., Kapur, T.: Confidence calibration and predictive uncertainty estimation for deep medical image segmentation. *IEEE transactions on medical imaging* **39**(12), 3868–3878 (2020)
- [41] Minderer, M., Djolonga, J., Romijnders, R., Hubis, F., Zhai, X., Houlsby, N., Tran, D., Lucic, M.: Revisiting the calibration of modern neural networks. *Advances in neural information processing systems* **34**, 15682–15694 (2021)
- [42] Mozafari, A.S., Gomes, H.S., Leão, W., Janny, S., Gagné, C.: Attended temperature scaling: a practical approach for calibrating deep neural networks. *arXiv preprint arXiv:1810.11586* (2018)
- [43] Niculescu-Mizil, A., Caruana, R.: Predicting good probabilities with supervised learning. In: Proceedings of the 22nd international conference on Machine learning. pp. 625–632 (2005)
- [44] Olsson, V., Tranheden, W., Pinto, J., Svensson, L.: Classmix: Segmentation-based data augmentation for semi-supervised learning. In: Proceedings of the IEEE/CVF Winter Conference on Applications of Computer Vision. pp. 1369–1378 (2021)
- [45] Park, S., Bastani, O., Weimer, J., Lee, I.: Calibrated prediction with covariate shift via unsupervised domain adaptation. In: International Conference on Artificial Intelligence and Statistics. pp. 3219–3229. PMLR (2020)
- [46] Peng, D., Hu, P., Ke, Q., Liu, J.: Diffusion-based image translation with label guidance for domain adaptive semantic segmentation. In: Proceedings of the IEEE/CVF International Conference on Computer Vision. pp. 808–820 (2023)
- [47] Pham, H., Dai, Z., Xie, Q., Le, Q.V.: Meta pseudo labels. In: Proceedings of the IEEE/CVF conference on computer vision and pattern recognition. pp. 11557–11568 (2021)
- [48] Platt, J., et al.: Probabilistic outputs for support vector machines and comparisons to regularized likelihood methods. *Advances in large margin classifiers* **10**(3), 61–74 (1999)
- [49] Richter, S.R., Vineet, V., Roth, S., Koltun, V.: Playing for data: Ground truth from computer games. In: Computer Vision–ECCV 2016: 14th European Conference, Amsterdam, The Netherlands, October 11–14, 2016, Proceedings, Part II 14. pp. 102–118. Springer (2016)
- [50] Ronneberger, O., Fischer, P., Brox, T.: U-net: Convolutional networks for biomedical image segmentation. In: Medical image computing and computer-assisted intervention–MICCAI 2015: 18th international conference, Munich, Germany, October 5–9, 2015, proceedings, part III 18. pp. 234–241. Springer (2015)
- [51] Ros, G., Sellart, L., Materzynska, J., Vazquez, D., Lopez, A.M.: The synthia dataset: A large collection of synthetic images for semantic segmentation of urban scenes. In: Proceedings of the IEEE conference on computer vision and pattern recognition. pp. 3234–3243 (2016)
- [52] Sakaridis, C., Dai, D., Van Gool, L.: Acdc: The adverse conditions dataset with correspondences for semantic driving scene understanding. In: Proceedings of the IEEE/CVF international conference on computer vision. pp. 10765–10775 (2021)
- [53] Salvador, T., Voleti, V., Iannantuono, A., Oberman, A.: Improved predictive uncertainty using corruption-based calibration. *stat* **1050**(7), 3 (2021)
- [54] Shen, F., Gurram, A., Liu, Z., Wang, H., Knoll, A.: Diga: Distil to generalize and then adapt for domain adaptive semantic segmentation. In: Proceedings of the IEEE/CVF Conference on Computer Vision and Pattern Recognition. pp. 15866–15877 (2023)
- [55] Tan, C., Sun, F., Kong, T., Zhang, W., Yang, C., Liu, C.: A survey on deep transfer learning. In: Artificial Neural Networks and Machine Learning–ICANN 2018: 27th International Conference on Artificial Neural Networks, Rhodes, Greece, October 4–7, 2018, Proceedings, Part III 27. pp. 270–279. Springer (2018)
- [56] Toldo, M., Michieli, U., Agresti, G., Zanuttigh, P.: Unsupervised domain adaptation for mobile semantic segmentation based on cycle consistency and feature alignment. *Image and Vision Computing* **95**, 103889 (2020)
- [57] Tomani, C., Gruber, S., Erdem, M.E., Cremers, D., Buettner, F.: Post-hoc uncertainty calibration for domain drift scenarios. In: Proceedings of the IEEE/CVF Conference on Computer Vision and Pattern Recognition. pp. 10124–10132 (2021)
- [58] Tranheden, W., Olsson, V., Pinto, J., Svensson, L.: Dacs: Domain adaptation via cross-domain mixed sampling. In: Proceedings of the IEEE/CVF Winter Conference on Applications of Computer Vision. pp. 1379–1389 (2021)
- [59] Tsai, Y.H., Hung, W.C., Schuster, S., Sohn, K., Yang, M.H., Chandraker, M.: Learning to adapt structured output space for semantic segmentation. In: Proceedings of the IEEE conference on computer vision and pattern recognition. pp. 7472–7481 (2018)
- [60] Wang, K., Kim, D., Feris, R., Betke, M.: Cdac: Cross-domain attention consistency in transformer for domain adaptive semantic segmentation. In: Proceedings of the IEEE/CVF International Conference on Computer Vision. pp. 11519–11529 (2023)
- [61] Wang, X., Long, M., Wang, J., Jordan, M.: Transferable calibration with lower bias and variance in domain adaptation. *Advances in Neural Information Processing Systems* **33**, 19212–19223 (2020)
- [62] Wei, D., Lin, Z., Franco-Barranco, D., Wendt, N., Liu, X., Yin, W., Huang, X., Gupta, A., Jang, W.D., Wang, X., et al.: Mitoem dataset: large-scale 3d mitochondria instance segmentation from em images. In: International Conference on Medical Image Computing and Computer-Assisted Intervention. pp. 66–76. Springer (2020)
- [63] Wu, Y., Shu, J., Xie, Q., Zhao, Q., Meng, D.: Learning to purify noisy labels via meta soft label corrector. In: Proceedings of the AAAI conference on artificial intelligence. vol. 35, pp. 10388–10396 (2021)
- [64] Xie, E., Wang, W., Yu, Z., Anandkumar, A., Alvarez, J.M., Luo, P.: Segformer: Simple and efficient design for semantic segmentation with transformers. *Advances in Neural Information Processing Systems* **34**, 12077–12090 (2021)
- [65] Yang, L., Hoyer, L., Weber, M., Fischer, T., Dai, D., Leal-Taixé, L., Pollefeys, M., Cremers, D., Van Gool, L.: Micdrop: masking image and depth features via complementary dropout for domain-adaptive semantic segmentation. In: European Conference on Computer Vision. pp. 329–346. Springer (2025)
- [66] Yin, D., Huang, W., Xiong, Z., Chen, X.: Class-aware feature alignment for domain adaptive mitochondria segmentation. In: International Conference on Medical Image Computing and Computer-Assisted Intervention. pp. 238–248. Springer (2023)
- [67] Yu, Y., Bates, S., Ma, Y., Jordan, M.: Robust calibration with multi-domain temperature scaling. *Advances in Neural Information Processing Systems* **35**, 27510–27523 (2022)
- [68] Yun, S., Han, D., Oh, S.J., Chun, S., Choe, J., Yoo, Y.: Cutmix: Regularization strategy to train strong classifiers with localizable features. In: Proceedings of the IEEE/CVF international conference on computer vision. pp. 6023–6032 (2019)
- [69] Zadrozny, B., Elkan, C.: Obtaining calibrated probability estimates from decision trees and naive bayesian classifiers. In: *Icml*. vol. 1 (2001)
- [70] Zhang, H., Cisse, M., Dauphin, Y.N., Lopez-Paz, D.: mixup: Beyond empirical risk minimization. *arXiv preprint arXiv:1710.09412* (2017)
- [71] Zhao, D., Wang, S., Zang, Q., Quan, D., Ye, X., Yang, R., Jiao, L.: Learning pseudo-relations for cross-domain semantic segmentation. In: Proceedings of the IEEE/CVF International Conference on Computer Vision. pp. 19191–19203 (2023)
- [72] Zou, Y., Deng, W., Zheng, L.: Adaptive calibrator ensemble: Navigating test set difficulty in out-of-distribution scenarios. In: Proceedings of the IEEE/CVF International Conference on Computer Vision. pp. 19333–19342 (2023)